Published in final edited form as:
Biomaterials. 2014 January ; 35(2): 825–835. doi:10.1016/j.biomaterials.2013.10.014.

Non-Viral DNA Delivery from Porous Hyaluronic Acid Hydrogels in Mice

Talar Tokatlian[1], **Cynthia Cam**[2], and **Tatiana Segura**[1,*]

[1]University of California, Los Angeles, Department of Chemical and Biomolecular Engineering

[2]University of California, Los Angeles, Department of Bioengineering

Abstract

The lack of vascularization within tissue-engineered constructs remains the primary cause of construct failure following implantation. Porous constructs have been successful in allowing for vessel infiltration without requiring extensive matrix degradation. We hypothesized that the rate and maturity of infiltrating vessels could be enhanced by complementing the open pore structure with the added delivery of DNA encoding for angiogenic growth factors. Both 100 and 60 μm porous and non-porous hyaluronic acid hydrogels loaded with pro-angiogenic (pVEGF) or reporter (pGFPluc) plasmid nanoparticles were used to study the effects of pore size and DNA delivery on angiogenesis in a mouse subcutaneous implant model. GFP-expressing transfected cells were found inside all control hydrogels over the course of the study, although transfection levels peaked by week 3 for 100 and 60 μm porous hydrogels. Transfection in non-porous hydrogels continued to increase over time corresponding with continued surface degradation. pVEGF transfection levels were not high enough to enhance angiogenesis by increasing vessel density, maturity, or size, although by 6 weeks for all pore size hydrogels more hydrogel implants were positive for vascularization when pVEGF polyplexes were incorporated compared to control hydrogels. Pore size was found to be the dominant factor in determining the angiogenic response with 60 μm porous hydrogels having more vessels/area present than 100 μm porous hydrogels at the initial onset of angiogenesis at 3 weeks. The results of this study show promise for the use of polyplex loaded porous hydrogels to transfect infiltrating cells in vivo and guide tissue regeneration and repair.

Keywords

Porous hydrogel; Controlled release; Non-viral gene delivery; Poly(ethylene imine); Subcutaneous implant

1. Introduction

Vascularization of tissue engineering constructs remains the primary reason for construct failure in vivo [1, 2]. Without the rapid infiltration of blood vessels, diffusion alone is insufficient to sustain migrating endogenous or exogenously implanted cells more than 150

*Corresponding Author: Tatiana Segura, Department of Chemical and Biomolecular Engineering, University of California, Los Angeles, 5531 Boelter Hall, 420 Westwood Plaza, Los Angeles, CA 90095-1592 (USA), tsegura@ucla.edu, Fax: 310-206-4107.

– 200 μm from the construct surface. Diffusion limitations then dictate the overall size and function of the implant, limiting their applicability in vivo to small injuries and defects [1, 3]. Thus, the promotion of angiogenesis (i.e. the formation of new vessels from pre-existing vessels) is essential for tissue engineering construct success. Efforts have already been made to promote angiogenesis within implanted hydrogels for soft tissue repair and regeneration through smart hydrogel design, hydrogel materials, and incorporation of pro-angiogenic growth factors and genes.

Over the past ten years, a major emphasis has been placed on macroscopic biomaterial design to help promote biomaterial vascularization. Patterning technologies, such as micro-contact printing, micro-molding, photolithography, micromachining, and laser-guided writing, have been used to form functional vascular structures inside biomaterials [4]. Although these patterning technologies allow for precise control over structure, issues with mass production has so far limited their clinical use. Alternatively, micro-scale interconnected pores produced through salt-leaching [5-7], gas foaming [8-10], lyophilization [11-14], and sphere templating [15-18] have shown to be effective in allowing for cellular migration in vitro [13, 19, 20] and tissue integration and, subsequent, enhanced scaffold vascularization in vivo [6, 16]. Chiu, et. al. demonstrated that increasing pore size from 25 to 150 μm in synthetic PEG hydrogels increased overall cellular infiltration and collagen deposition, as well as vascular infiltration from the surrounding tissue into the pores of the PEG hydrogel [6]. Similarly Madden, et. al. incorporated both spherical pores as well as channels into poly(2-hydroxyethyl methacrylate-co-methacrylic acid) hydrogels which were shown to significantly enhance neovascularization 4 weeks after myocardial implantation [16]. However, they demonstrated that scaffold architecture influenced macrophage polarity and that an intermediate pore size of 30-40 μm lead to increased neovascularization as a result of a shift in macrophages in the M1 pro-inflammatory phase to macrophages in the M2 pro-healing (anti-inflammatory) stage. In all of these reports, pore size was found to play a crucial role in the rate of angiogenesis and the size and maturity of the formed vessels.

The type of natural (i.e. collagen, alginate, chitosan, hyaluronic acid (HA)) or synthetic (i.e. poly(ethylene glycol), poly(ethylene oxide), poly(vinyl alcohol), poly(acrylic acid), polypeptides) polymer used for hydrogel preparation is an important factor in determining cell-material interactions, mechanical properties, fluid permeability and, subsequently, promotion of angiogenesis [2, 11, 21, 22]. While a synthetic polymer, such as PEG, can be biochemically inert, natural polymers possess intrinsic qualities which can play a role in signaling to surrounding cells. HA, an anionic, non-sulfated glycosaminoglycan and major component of the ECM, has gained popularity as a biomaterial for tissue engineering and regeneration due to its high biocompatibility and low immunogenicity [23-26]. Moreover, degraded fragments of HA or HA oligomers are known to promote angiogenesis and up-regulate MMP expression [27-29]. HA specifically interacts with cell surface receptors, such as CD44, RHAMM (receptor for HA mediated motility) and ICAM-1 (intercellular adhesion molecule 1), and contributes to tissue hydrodynamics, cell proliferation and migration [30, 31]. Using mild chemistries the HA backbone can be modified to contain functional groups, such as thiols, acrylates or amines, which can be further used as crosslinking sites to form hydrogels [25, 32-34]. As a result, several studies have demonstrated that HA-based hydrogels are good candidates for culturing stem cells [35-38]. Semi-synthetic hyaluronic acid (HA) hydrogels which are degradable by hyaluronidases as well as matrix metalloproteinases (MMPs) via MMP-degradable peptide crosslinkers have previously been developed for culturing mouse mesenchymal stem cells in 3-dimensions [39, 40]. MMPs are normally expressed during tissue remodeling and are up-regulated during wound healing, microenvironment remodeling, and in diseased states and can, therefore, serve as triggers for bioactive signal delivery.

The effective local delivery of angiogenic factors, including vascular endothelial growth factor (VEGF) and platelet derived growth factor (PDGF), are necessary to promote blood vessel formation. While peptides and growth factors can be easily incorporated within these hydrogels, rapid degradation by proteases generally limits their effectiveness in long-term cell culture. For tissue regeneration, localized gene delivery can promote the expression of tissue inductive factors to guide tissue formation. Poly(ethylene imine) (PEI) is the most widely utilized cationic polymer for non-viral gene delivery; it is able to condense DNA through electrostatic interactions between the positively charged amines on the PEI and the negatively charged phosphates on the DNA, forming nanoparticles (polyplexes) in the range of 50 to 200 nm [41-43]. PEI has been successfully used in vivo to deliver DNA or siRNA to the brain [44, 45], lungs [46-50], abdomen [51], liver [52], and tumors [53-55]. DNA/PEI polyplexes have also been incorporated into fibrin [17, 56], alginate [57], gelatin [58], and other natural polymer based hydrogels [59]. Researchers have likewise utilized enzymatically degradable synthetic polymer scaffolds, which release their payload upon cellular infiltration [60-62]. Since then MMP-degradable hyaluronic acid hydrogels have also been used to encapsulate DNA/poly(PEI) polyplexes as a means of non-viral gene delivery to stem cells [63]. We found that as the matrix degraded through cell-secreted proteases, the cells were transfected with the polyplexes encountered during their migration. DNA polyplexes can also be loaded at therapeutically relevant concentrations (≥1 μg/μL) using a caged nanoparticle encapsulation process (CnE) inside a variety of hydrogel scaffolds without particle aggregation [64, 65]. This approach utilizes neutral saccharides (sucrose) and polysaccharides (agarose) to protect the polyplexes from inactivation and aggregation during lyophilization and hydrogel formation, respectively.

Since the emergence of non-viral gene delivery from hydrogel scaffolds, emphasis has been placed on complementing gene transfer with matrix design to enhance transfection efficiency. Micron-sized pores is one key factor which has shown to increase both viral [66] and non-viral [8, 9, 17] gene transfer by increasing the available surface area for cells to degrade the biomaterial and release the encapsulated signal. We previously investigated gene transfer to mouse mesenchymal stem cells (mMSCs) seeded within porous hyaluronic acid hydrogel scaffolds in vitro [67]. Using the CnE process to incorporate DNA/PEI polyplexes, porous hydrogels allowed for sustained transfection and transgene expression of incorporated mMSCs in various pore size hydrogels. For all investigated pore sizes transgene expression was sustained for up to ten days. We anticipated that the presence of an open pore structure would increase the rate of vascularization through enhanced cellular infiltration into the gel and that the added delivery of DNA encoding for angiogenic growth factors would result in long lasting angiogenic signals. Here we describe the results when this hydrogel system was used to deliver DNA in vivo in a mouse subcutaneous implant model.

2. Materials and Methods

2.1 Materials

Peptides Ac-GCRDGPQGIWGQDRCG-NH2 (HS-MMP-SH) and Ac-GCGYGRGDSPG-NH2 (RGD) were purchased from Genscript (Piscataway, NJ). Sodium hyaluronan (HA) was a gift from Genzyme Corporation (60 kDa, Cambridge, MA). Linear poly(ethylene imine) (PEI, 25 kDa) was purchased from Polysciences (Warrington, PA). Vectors expressing mammalian GFP-firefly luciferase (pGFPluc) and human VEGF-165 (pVEGF) were obtained from New England Biolabs (Ipswich, MA) and expanded using a Giga Prep kit from Qiagen following the manufacturer's protocol. All other chemicals were purchased from Fisher Scientific (Pittsburgh, PA) unless otherwise noted.

2.2 Hyaluronic acid modification

Sodium hyaluronan was modified to contain acrylate functionalities. Briefly, hyaluronic acid (2.00 g, 60kDa, 5.28 mmol carboxylic acids) was reacted with 36.77 g (211.07 mmol) adipic acid dihydrazide (ADH) at pH 4.75 in the presence of 4.00 g (20.84 mmol) 1-ethyl-3-[3-dimethylaminopropyl] carbodiimide hydrochloride (EDC) overnight and purified through dialysis (8000 MWCO) in a 100 mM to 0 mM salt gradient for 1 day followed by dialysis in DI water for 4-5 days. The purified intermediate (HA-ADH) was lyophilized and stored at −20 °C until used. Approximately 54 % of the carboxyl groups were modified with ADH, which was determined using ^{1}H NMR (D_2O) by taking the ratio of peaks at δ = 1.6 and 2.3 corresponding to the 8 hydrogens of the methylene groups on the ADH to the singlet peak of the acetyl methyl protons in HA (δ = 1.88). All of the modified HA-ADH was reacted with N-Acryloxysuccinimide (NHS-Ac) (4.46 g, 26.38 mmol) in HEPES buffer (10 mM HEPES, 150 mM NaCl, 10 mM EDTA, pH 7.2) overnight and purified through dialysis in a 100 mM to 0 mM salt gradient for 1 day followed by dialysis in DI water for 3-4 days before lyophilization. The degree of acrylation was determined to be ∼12 % using 1H-NMR (D_2O) by taking the ratio of the multiplet peak at δ = 6.2 corresponding to the cis and trans acrylate hydrogens to the singlet peak of the acetyl methyl protons in HA (δ = 1.88).

2.3 Polyplex lyophilization

For CnE, plasmid DNA (250 μg) and L-PEI (228.3 μg, N/P = 7) were mixed in 3.5 mL water in the presence of 35 mg (0.10 mmol) of sucrose (Ultra pure, MP Biomedicals, Santa Ana, CA) and incubated at room temperature for 15 min. Low-melting point agarose (1.0 mg, UltraPureTM Agarose, Tm = 34.5-37.5 °C, Invitrogen, Grand Islands, NY) in 1.5 mL water was added before lyophilization. Each aliquot was intended for a 100 μL hydrogel. For smaller hydrogel volumes, both sucrose and agarose were scaled down proportionally.

2.4 Design template using PMMA microspheres

Microsphere templates for porous hydrogels were prepared using dry PMMA microspheres (27-33, 53-63, and 90-106 μm, Cospheric, Santa Barbara, CA). Approximately 20 mg of microspheres (1.19 mg/μL) were mixed with DI water for a final concentration of 20 mg per 100 μL. Then 100 μL of the microsphere solution was pipetted into each well in a glass-bottom silicon well mold (wells = 6 mm × 2 mm, D × H). The microspheres were then allowed to dry and pack (by naturally settling) over 3-4 h at 37 °C. The glass-bottom silicon wells were then placed into an oven and the microspheres were sintered for 22 h at 150 °C.

2.5 Porous (and non-porous) HA hydrogel formation

Hydrogels were formed by Michael-type addition of acrylate-functionalized HA (HA-Ac) with bis-cysteine containing MMP peptide crosslinkers at pH 8.0-8.2. Prior to reaction, a hydrogel precursor solution was made by mixing a fraction of the total HA-Ac with a lyophilized aliquot of cell adhesion peptide, RGD, in .3 M TEOA pH 8.2 for 30 min at 37 °C. After incubation, HA-RGD was mixed with the remaining HA-Ac and .3 M TEOA pH 8.2 for a final gel concentration of 3.0 w/v% HA and 100 μM RGD. Finally lyophilized aliquots of the crosslinker (HS-MMP-SH) were diluted in .3 M TEOA pH 8.2 immediately before addition to a mixture of lyophilized (CnE) DNA/PEI polyplexes and the hydrogel precursor solution for a final r ratio (SH/Ac) = 0.4. For porous hydrogels, 20 μL of gel solution was then added directly on top of a PMMA microsphere template, covered with a glass slide, and perfused into the template by centrifugation at 1500 rpm for 6 min at 4 °C. The slide was then incubated at 37 °C for 30-45 min to induce polymerization. Once complete, the gels were removed from the silicon wells and placed directly into 100 % acetone for 48 h to dissolve the PMMA microsphere template. The acetone solution was replaced 2-3× during this incubation. The gels were then serially hydrated into sterile PBS

and left in PBS until ready for use. For non-porous hydrogels, the gel solution was sandwiched between two Sigmacoted slides using 1 mm thick plastic spacers and incubated at 37 °C for 30-45 min to induce polymerization. Once complete, the gels were placed directly into sterile PBS and left in PBS until ready for use. Prior to surgery all gels were placed in sterile PBS with 1 % P/S overnight.

Plate-to-plate rheometry was used to determine the mechanical properties of the hydrogels with an Anton Parr rheometer under a constant strain of 0.01 and frequency range of 0.1-10 Hz. The mesh size of non-porous hydrogels was determined using the following equations based on the Rubber Elasticity and Flory-Rehner theories:

$$Molecular\ weight\ between\ crosslinks \quad M_{XL} = \frac{\rho RT}{G}$$

$$Correlation\ distance\ between\ crosslinks \quad \xi = L\left(\frac{2C_n M_{XL}}{M_r}\right)^{\frac{1}{2}} v_{2,s}{}^{-\frac{1}{3}}$$

where M_{xl} is the molecular weight between crosslinks, ρ is the polymer density in the hydrogel, R is the universal gas constant, T is the absolute temperature, G is the average storage modulus, ξ is the correlation distance between crosslinks (i.e. mesh size), L is the length of the bond along the polymer backbone, C_n is Flory characteristic ratio for the polymer, M_r is the molecular weight of the polymer's repeating units, and $v_{2,s}$ is the swollen polymer volume fraction.

2.6 Subcutaneous implant model

All in vivo studies were conducted in compliance with the NIH Guide for Care and Use of Laboratory Animals and UCLA ARC standards. 6 to 8-week old female Balb/c mice each 20-30 grams were used to study cellular infiltration and blood vessel formation in HA hydrogels since this strain and size has been previously used for wound healing and angiogenesis assays [68, 69]. Porous and non-porous hydrogels were made exactly as described above and cut to 6 mm in diameter using a biopsy punch, for final overall dimensions of 6 mm × 1 mm, D × H. In fabricating the hydrogels, the starting reagents were sterilized through filtering with a 0.22 μm filter. After scaffold fabrication, the hydrogels were washed with sterile PBS and kept in PBS with 1 % P/S. Immediately prior to surgery, mice were anesthetized with 4-5 % isoflurane through a nose cone inhaler. After anesthesia induction, the isoflurane concentration was lowered to 1.5-2.5 % for the remainder of the surgery. The back of the mouse was subsequently shaved and washed with Betadine and 70 % ethanol. Two incisions appropriate to the size of the implant were made in the skin aside the midline of the animal using scissors. Two subcutaneous pockets were subsequently created by blunt dissection using hemostats. Within the created pockets, the implants were inserted. After insertion of the hydrogels, each incision was subsequently closed with a single wound clip. All animals were observed daily for signs of inflammation and pain and also administered Carprofen injections for the first 48 h post survival surgery. Mice (n = 4) were sacrificed after 1, 3, and 6 weeks with isoflurane overdose. Two 1 cm^2 pieces of tissue were collected from each mouse containing the implant and the surrounding tissue and skin, fixed in 2 % PFA overnight at 4 °C, dehydrated in 70 % EtOH, and finally paraffin embedded.

2.7 Immunofluorescence and immunohistochemistry

Paraffin embedded sections (5 μm) were deparaffinized by incubation in multiple xylene washes followed by serial hydration from 100 % ethanol into 100 % water. For CD31/α-SMA staining, antigen-retrieval was conducted with a 15 min incubation at 37 °C in 0.1 mg/mL proteinase K solution. Sections were then washed with PBS and incubated in blocking buffer (1 % goat serum (Invitrogen, Grand Islands, NY) + 0.05 % Tween-20 in PBS) for 1 h at RT before being incubated in primary antibody solution (1:100 dilution in blocking buffer of rat anti-mouse CD31 (BD Pharmingen, San Diego, CA)) overnight at 4 °C. Sections were again washed with PBS and incubated in blocking buffer for 10 min at RT before being incubated for 2 h at RT in secondary antibody solution (1:100 dilution in blocking buffer of goat anti-rat Alexa 568 (Invitrogen, Grand Islands, NY) which also contained α-smooth muscle actin-FITC (1:100 dilution, Sigma-Aldrich, St. Louis, MO) and DAPI nuclear stain (1:400 dilution, Invitrogen). Sections were then washed twice in PBS, mounted and imaged using an inverted Zeiss fluorescence microscope. For GFP staining, neither protease nor heat-mediated antigen-retrieval was conducted as these were found to eliminate any GFP signal. All other procedures were conducted exactly as described above with a 1:50 dilution of the primary GFP antibody (Invitrogen, Grand Islands, PA) and 1:100 and 1:400 dilutions of the goat anti-rabbit Alexa 488 secondary antibody (Invitrogen, Grand Islands, PA) and DAPI, respectively. All hematoxylin and eosin staining of sections was conducted by the Translational Pathology Core Laboratory (TPCL) at UCLA.

2.8 GFP characterization and statistical analysis

Two separate sections at least 50 – 100 μm apart were analyzed for each implant. Twenty randomly chosen areas were imaged from each section. ImageJ software was used to quantify GFP positive signal (GFP+ pixels/ total pixels). An average of several images from pVEGF containing implants were used to determine a background threshold to account for tissue auto-fluorescence. GFP positive signal was then normalized to number of cells per image (acquired through DAPI channel). The bar graph in Figure 4J represents the average % GFP+ area/cells from 4 different implants (i.e. animals).

All statistical analysis was performed using Prism (GraphPad, San Diego, CA). Experiments were statistically analyzed using a one-way ANOVA followed by a Tukey test to compare all pairs of columns using a 95 % confidence interval. All error bars represent the standard error of the mean (SEM).

2.9 Vessel quantification, characterization, and statistical analysis

Three separate sections at least 100 – 150 μm apart were analyzed for each implant. Ten randomly chosen areas were imaged in each section. Vessels were counted manually in each section, totaled from all 30 sections, and finally normalized to the total imaged area. The bar graph in Figure 6A represent the average vessels/mm^2 from 4 different implants (i.e. animals). For hydrogel implants that contained a minimum of at least 15 vessels/mm^2 (i.e. at least 1 vessel in 50 % of captured images, designated by dotted red line in Figure 5A), the diameter of each vessel was manually measured using Zen imaging and analysis software (Zeiss). Percentages were determined using the entire vessel set.

All statistical analysis was performed using Prism (GraphPad, San Diego, CA). Experiments were statistically analyzed using either a one-way ANOVA for similar groups of samples (e.g. all pore size hydrogels at week 1) or a t-test followed by a Tukey test to compare all pairs of columns using a 95 % confidence interval. All errors bars represent the standard error of the mean (SEM).

3. Results

Utilizing the CnE process of polyplex encapsulation, polyplexes were incorporated at a concentration of 2.5 μg/μL into 100 and 60 μm porous and non-porous (n-pore) hydrogels and implanted subcutaneously into the backs of Balb/c mice. Each mouse had implanted a pVEGF containing gel and its respective pGFPluc loaded control. Single-phase porous and n-pore hydrogels were prepared as previously described [67]. Hydrogel implants were excised and analyzed at 1, 3, and 6 weeks. These time points were strategically chosen in order to observe initial differences in cellular infiltration (week 1), initial appearances of small capillaries and other small vessels (week 3), and sustained presence of new vasculature (week 6). Hematoxylin and eosin (H&E) staining of hydrogel cross-sections indicated increasing cellular infiltration with time and porosity (Figure 1). At week 1, 100 μm porous hydrogels seemed to have the most infiltration as well as ECM deposition into the pores. No distinguishable differences could be observed between 100 and 60 μm porous hydrogels at 3 and 6 weeks. Importantly, there were no visible differences in infiltration in hydrogels loaded with pVEGF or pGFPluc loaded polyplexes. Small vessels perfused with erythrocytes (i.e. red blood cells) could be observed in 100 and 60 μm porous hydrogels at 3 and 6 weeks. No vessels seemed to be present in n-pore hydrogels by 6 weeks even though hydrogel degradation, and subsequent polyplex release, did continue to increase over time. Importantly, no fibrous capsule or inflammatory tissue could be observed surrounding any of the hydrogel implants (Figure 2). No foreign body giant cells could be observed.

Immunofluorescence staining for GFP in pGFPluc loaded control hydrogels indicated that transfected cells were present in each hydrogel over the course of the study (Figure 3), although the number of transfected cells within the pores of 60 μm porous hydrogels was significantly higher than the number of transfected cells within the pores of 100 μm porous and n-pore hydrogels at 1 week (Figure 3J). By 3 weeks, there was no statistical difference between the levels of transfection between 60 and 100 μm porous hydrogels. In contrast, at all times there was a statistically higher number of transfected cells within the pores of 60 μm porous hydrogels compared to n-pore hydrogels (note: 100 μm hydrogels only contained a statistically higher number of transfected cells compared to n-pore hydrogels at 3 and 6 weeks). Although the overall levels of GFP expression were much lower, the number of transfected cells in n-pore hydrogels continued to steadily increase with time as a direct result of continued cellular infiltration and hydrogel degradation (Figure 3C, F, I).

To determine if the degree of transfection observed led to an enhancement in angiogenesis in pVEGF loaded hydrogels, all implants were analyzed by immunofluorescence for PECAM positive endothelial cells. The difference in angiogenesis between porous and n-pore hydrogels, similar to what was observed in the preliminary in vivo study without incorporated polyplexes [67], was clear from both H&E stained sections and visible vessels which could be observed directly within the implants by visual inspection upon excision (Figure 4). Upon staining for PECAM positive endothelial cells and smooth muscle cells, capillaries and other small vessels were found to be present in only a fraction of pVEGF (Figure 5A, G) and pGFPluc (Figure 5D, J) loaded 100 μm porous hydrogels at 3 and 6 weeks, respectively. For 60 μm porous hydrogels, all implants had vessels present at 3 weeks while only a fraction of pVEGF (Figure 5H) and pGFPluc (Figure 5K) implants were vascularized at 6 weeks. As expected, no vessels were observed in either pVEGF (Figure 5C) or pGFPluc (Figure 5F) loaded n-pore hydrogels at 3 weeks. However, detailed staining revealed some small vessels in the degraded gel area surrounding the bulk hydrogel in about half of pVEGF (Figure 5I) and pGFPluc (Figure 5L) loaded n-pore hydrogels at 6 weeks. For all conditions, hydrogels from week 1 were not further analyzed for angiogenesis since no vessels could be observed from H&E stained sections.

For further validation of observed differences, vessels in 3 separate sections of each hydrogel implant (n = 3-4) were quantified and represented as averages ± SEM in Figure 6A. Those hydrogels that contained only a few, but still less than 15 vessels/mm^2, fell below the dotted red line. A summary of all hydrogel implants positive for PECAM positive blood vessels is found in Table 1. Importantly, for all pore size hydrogels loaded with pVEGF polyplexes at 6 weeks more implants were positive for vessels when compared to corresponding hydrogels loaded with pGFPluc polyplexes. Quantification of vessel density further revealed, as expected, that all n-pore hydrogels had significantly fewer vessels present than their corresponding 60 μm porous hydrogels at 3 weeks. However, only in the absence of VEGF delivery (i.e. in pGFPluc loaded hydrogels) was there a significant difference between the 60 and 100 μm porous hydrogels, with the 60 μm gels having significantly higher vessel density at 3 weeks. Mechanical testing of these porous hydrogels later revealed that, although the hydrogel composition between gel types remained constant, the overall gel modulus was largely influenced by the presence of pores and pore size (Figure 7). The observed differences in vasculature between the 60 and 100 μm porous hydrogels could then be, at least in part, attributed to the differences in mechanical properties. On the other hand, by 6 weeks there were no statistical differences between any hydrogel types. Finally, it was revealed that the 60 μm porous hydrogels that had the highest average number of vessels per area at 3 weeks were the only ones to have a significant reduction in vessels by 6 weeks (i.e. vessel regression). This vessel regression was not observed, however, for pVEGF loaded 60 μm porous gels. Most importantly, at no time was there any significant increase in the number of vessels per area between pVEGF and corresponding pGFPluc loaded hydrogels. Thus, any VEGF that was being expressed was not at a high enough level to induce an angiogenic response, but may have been enough to sustain vessels that had already formed as a result of the open pore structure.

All sections were also stained directly for smooth muscle cells to assess vessel maturity as a function of VEGF expression and pore size (Figure 5). No smooth muscle actin staining was observed surrounding vessels within any hydrogel cross-sections. To characterize vessel size distribution, the diameters of all vessels in hydrogel implants that were positive for blood vessels were manually measured. Vessels from hydrogels that fell below this threshold were not included in the vessel size characterization analysis to prevent biasing by a few large vessels. It was clear that in all hydrogel implants about 40-60 % of all vessels were <6 μm in diameter, or the width of a single red blood cell, both at 3 (Figure 6B) and 6 (Figure 6C) weeks.

4. Discussion

Vascular endothelial growth factor (VEGF) is a known initiator of vessel branching and angiogenesis and the controlled delivery of VEGF both in vitro and in vivo has been shown to enhance angiogenic responses when compared to a single bolus delivery [70-74]. While growth factor delivery remains the primary method to promote angiogenesis in vivo, the process of porous hydrogel formation using a sphere-template approach involves harsh solvents, which are not suitable for growth factor encapsulation. As an alternative, non-viral plasmid DNA can be delivered to transfect infiltrating cells to produce the protein(s) of interest. The work described here aims to deliver pro-angiogenic pVEGF polyplexes to infiltrating cells from a protease-degradable, porous hydrogel in vivo to promote sustained blood vessel infiltration.

In general, when growth factors (and, likewise, other small nanoparticles or small molecules) are encapsulated into hydrogel scaffolds, their release is dictated by diffusion out of the gel and gel degradation kinetics. For those gels with agarose and sucrose, the storage modulus of 3 % HA hydrogels (non-porous) with 0.4 – 0.6 r-ratios (SH/Ac) can range from

100 – 400 Pa. This range corresponds to ∼770 – 190 kg/mol between crosslinks and approximately 60 – 30 nm mesh size, respectively, as determined by the Rubber Elasticity and Flory–Rehner theories [75]. These hydrogels are termed non-porous (n-pore). Thus, for large polyplexes and DNA nanoparticles (>80 nm) hydrogel mesh size generally limits diffusion and requires that the gel degrade in order for release of encapsulated nanoparticles to occur. The same holds true for porous hydrogels, although porous hydrogels have a much higher available surface area for cells to be able to degrade and release encapsulated polyplexes. H&E stained sections of 100 and 60 μm porous (theoretical porosity for hexagonal close-packed bead template = 76 %, actual porosity = 45 – 65 %) and n-pore hydrogels at 1, 3, and 6 weeks demonstrates the differences in infiltration and overall hydrogel degradation as a result of porosity (Figure 1). Initially a higher degree of infiltration was observed for the largest pore size, similar to what was reported for porous PEG hydrogels with comparable pore sizes [6]. This qualitative difference diminished by 3 weeks when most of the pores in both 100 and 60 μm porous hydrogels were extensively infiltrated.

Since no visible differences could be seen between hydrogels loaded with pVEGF or pGFPluc polyplexes, it became crucial to determine if the released polyplexes were in fact able to transfect infiltrating cells in vivo and, if so, to what extent these cells were being transfected. All pGFPluc loaded hydrogel implants were positive for GFP-transfected cells (Figure 3). Porous hydrogels contained the highest number of transfected cells within their pores at approximately 3 weeks, while the number of transfected cells continued to increase through the 6-week period in the outer degrading edge of the n-pore hydrogels. This may be reflective of the degree of hydrogel degradation between 1 and 3 weeks and 3 and 6 weeks. We hypothesized that if after 3 weeks cells which had already infiltrated the scaffold become quiescent as a result of minimal immune response to the natural hydrogel material and slowly released polyplexes (i.e. low pDNA/PEI concentration at any given time), degradation of the surrounding matrix and release and transfection of entrapped polyplexes could potentially slow down. The number of transfected cells in n-pore hydrogels, however, continued to increase over time as a clear result of continuous gel degradation allowing for exposure to fresh polyplexes. This was similar to the continuous transfection observed for cell clots encapsulated inside n-pore hydrogels loaded with polyplexes in vitro in which transfection was sustained for up to 21 days [61]. Transfected cells in n-pore hydrogels, thus, were only located around the hydrogel periphery where there was continuous infiltration and gel degradation, while transfected cells in 100 and 60 μm porous gels could be found throughout internal pores.

Direct staining for endothelial cells showed clearly that capillaries and other small vessels were present in porous HA hydrogels at 3 weeks (Figure 5). The results of the vessel quantification (Figure 6A, Table 1), however, revealed several things that were not directly apparent from the immunofluorescence images. In general, all 60 μm porous hydrogel implants were vascularized by 3 weeks regardless of VEGF expression. For pGFPluc loaded hydrogels, 60 μm porous hydrogels had a significantly higher number of vessels per cross-sectional area than 100 μm porous hydrogels at 3 weeks. This was not the case for pVEGF loaded porous hydrogels at 3 weeks. It was unclear, however, whether the reason there was no significant difference between the 100 and 60 μm pVEGF loaded hydrogels was, in fact, due to VEGF expression or if variability among the 100 μm implants muddled potential differences. One hypothesis is that 60 μm porous gels have more vessels/area than 100 μm porous gels because the bulk storage modulus is significantly lower for the 60 μm porous gels compared to the 100 μm porous gels of the same hydrogel composition (Figure 7), making them more conducive for cellular infiltration and hydrogel degradation. Along the same lines, at the cellular level the smaller, interconnected pores of the 60 μm porous hydrogels create more rigid and clear channels for vessels to extend through. The pores in

the 100 μm porous hydrogels, especially when using a soft hydrogel material containing only 3 % HA, are much more deformable. Potentially a more rigid local structure can help guide angiogenesis in its initial stages. It is important to note that vessels were only present in regions of the gels that were infiltrated. Thus, in n-pore hydrogel implants, all the vessels that were present were located around the gel edge in the degraded gel regions and not in the bulk gel. The distribution of vessels was similar to the distribution of transfected cells. By 6 weeks expression of VEGF seemed to play a more significant role as all pore size hydrogels loaded with pVEGF polyplexes had more hydrogel implants positive for vascularization (> 15 vessels/mm^2) compared to their corresponding pGFPluc loaded control hydrogels (Table 1). Yet no statistical significance could be observed between the overall vascular densities between any hydrogel types at this time (Figure 6A).

Finally, if VEGF expression had been too low to affect the number of vessels infiltrating the scaffold, there was still a possibility that VEGF expression could have affected vessel maturity and size. Pericyte or smooth muscle cell lining is one indicator of vessel maturity [2, 70, 76]. All vessels found within the hydrogel pores, however, were negative for smooth muscle cells. This suggested that incorporation of additional factors, such as platelet-derived growth factor (PDGF), might be necessary to promote vessel maturation. There were also no striking differences in vessel size between pVEGF and corresponding pGFPluc loaded hydrogels (Figure 6B, C). Since the number of vessel-positive hydrogel implants in certain gel conditions was low (i.e. only 1 or 2), further statistical analysis could not be performed.

5. Conclusions

Porous and n-pore HA hydrogels loaded with pro-angiogenic (pVEGF) or reporter (pGFPluc) plasmids were tested for their ability to induce an enhanced angiogenic response by transfecting infiltrating cells in vivo. Although GFP-expressing transfected cells were present inside all hydrogel implants over the 6-week study, transfection levels peaked around week 3 for 100 and 60 μm porous hydrogels while it continued to increase along with continued gel degradation in n-pore hydrogels. Although by 6 weeks for all pore size hydrogels more hydrogel implants were vessel-positive when pVEGF polyplexes were incorporated compared to corresponding control hydrogels, transfection levels of pVEGF still did not seem to be high enough to enhance angiogenesis by significantly increasing vessel density, maturity, or size. Only in 60 μm porous hydrogels did VEGF expression play a role in preventing vessel regression and helping to sustain the number of vessels present from 3 to 6 weeks. Regardless, pore size seemed to be the dominant factor in determining the angiogenic response, with 60 μm porous hydrogels having more vessels present per area than 100 μm porous hydrogels at the initial onset of angiogenesis at 3 weeks. Increased pore rigidity may have been a key factor. Combined these results, show promise for the use of polyplex loaded porous hydrogels to transfect infiltrating cells in vivo and guide tissue regeneration and repair.

Acknowledgments

The authors would like to thank Dr. Joanne Zahorsky-Reeves and Dr. Joanne Sohn for their continuous help with the animal models, as well as Dr. Lloyd Miller for technical support with histology and Dr. David Gjertson for assistance with statistical analysis. T. Tokatlian would especially like to thank Suwei Zhu, Shayne Siegman, Shiva Gojgini, and Dr. Lina Nih for their assistance at one point or another with the animal experiments and Dr. Antoni Torres Collado for his advice and helpful discussions. The authors acknowledge the NIH (R01HL110592), NSF (CAREER 0747539), and CRCC for funding this work.

References

1. Novosel EC, Kleinhans C, Kluger PJ. Vascularization is the key challenge in tissue engineering. Adv Drug Deliv Rev. 2011; 63:300–11. [PubMed: 21396416]

2. Bramfeldt H, Sabra G, Centis V, Vermette P. Scaffold vascularization: a challenge for three-dimensional tissue engineering. Curr Med Chem. 2010; 17:3944–67. [PubMed: 20939827]
3. Laschke MW, Menger MD. Vascularization in tissue engineering: angiogenesis versus inosculation. Eur Surg Res. 2012; 48:85–92. [PubMed: 22456224]
4. Papavasiliou G, Cheng MH, Brey EM. Strategies for vascularization of polymer scaffolds. J Investig Med. 2010; 58:838–44.
5. Chiu Y, Larson J, Isom AJ, Brey E. Generation of porous poly(ethylene glycol) hydrogels by salt leaching. Tissue Eng Part C Methods. 2010; 16:905–12. [PubMed: 19905877]
6. Chiu YC, Cheng MH, Engel H, Kao SW, Larson JC, Gupta S, et al. The role of pore size on vascularization and tissue remodeling in PEG hydrogels. Biomaterials. 2011; 32:6045–51. [PubMed: 21663958]
7. Huang X, Zhang Y, Donahue H, Lowe T. Porous thermoresponsive-co-biodegradable hydrogels as tissue-engineering scaffolds for 3-dimensional in vitro culture of chondrocytes. Tissue Eng. 2007; 13:2645–52. [PubMed: 17683245]
8. Huang YC, Riddle K, Rice KG, Mooney DJ. Long-term in vivo gene expression via delivery of PEI-DNA condensates from porous polymer scaffolds. Hum Gene Ther. 2005; 16:609–17. [PubMed: 15916485]
9. Jang JH, Rives CB, Shea LD. Plasmid delivery in vivo from porous tissue-engineering scaffolds: transgene expression and cellular transfection. Mol Ther. 2005; 12:475–83. [PubMed: 15950542]
10. Nam YS, Yoon JJ, Park TG. A novel fabrication method of macroporous biodegradable polymer scaffolds using gas foaming salt as a porogen additive. J Biomed Mater Res. 2000; 53:1–7. [PubMed: 10634946]
11. Iyer P, Walker KJ, Madihally SV. Increased matrix synthesis by fibroblasts with decreased proliferation on synthetic chitosan–gelatin porous structures. Biotechnol Bioeng. 2011; 109:1314–25. [PubMed: 22125268]
12. Kang HW, Tabata Y, Ikada Y. Fabrication of porous gelatin scaffolds for tissue engineering. Biomaterials. 1999; 20:1339–44. [PubMed: 10403052]
13. Kang JY, Chung CW, Sung JH, Park BS, Choi JY, Lee SJ, et al. Novel porous matrix of hyaluronic acid for the three-dimensional culture of chondrocytes. Int J Pharm. 2009; 369:114–20. [PubMed: 19059468]
14. Van Vlierberghe S, Cnudde V, Masschaele B, Dubruel P, De Paepe I, Jacobs PJS, et al. Porous gelatin cryogels as cell delivery tool in tissue engineering. J Control Release. 2006; 116:e95–e8. [PubMed: 17718993]
15. Galperin A, Long TJ, Ratner BD. Degradable, thermo-sensitive poly(n-isopropyl acrylamide)-based scaffolds with controlled porosity for tissue engineering applications. Biomacromolecules. 2010; 11:2583–92. [PubMed: 20836521]
16. Madden LR, Mortisen DJ, Sussman EM, Dupras SK, Fugate JA, Cuy JL, et al. Proangiogenic scaffolds as functional templates for cardiac tissue engineering. Proc Natl Acad Sci U S A. 2010; 107:15211–6. [PubMed: 20696917]
17. Saul JM, Linnes MP, Ratner BD, Giachelli CM, Pun SH. Delivery of non-viral gene carriers from sphere-templated fibrin scaffolds for sustained transgene expression. Biomaterials. 2007; 28:4705–16. [PubMed: 17675152]
18. Stachowiak AN, Bershteyn A, Tzatzaloz E, Irvine DJ. Bioactive hydrogels with an ordered cellular structure combine interconnected macroporosity and robust mechanical properties. Adv Mater. 2005; 17:399–403.
19. Peyton SR, Kalcioglu ZI, Cohen JC, Runkle AP, Van Vliet KJ, Lauffenburger DA, et al. Marrow-derived stem cell motility in 3D synthetic scaffold is governed by geometry along with adhesivity and stiffness. Biotechnol Bioeng. 2011; 108:1181–93. [PubMed: 21449030]
20. Stachowiak AN, Irvine DJ. Inverse opal hydrogel-collagen composite scaffolds as a supportive microenvironment for immune cell migration. J Biomed Mater Res A. 2008; 85:815–28. [PubMed: 17937415]
21. Andreadis ST, Geer DJ. Biomimetic approaches to protein and gene delivery for tissue regeneration. Trends Biotechnol. 2006; 24:331–7. [PubMed: 16716420]

22. Fischbach C, Mooney DJ. Polymers for pro- and anti-angiogenic therapy. Biomaterials. 2007; 28:2069–76. [PubMed: 17254631]
23. Leach JB, Bivens KA, Patrick CW, Schmidt CE. Photocrosslinked hyaluronic acid hydrogels: natural, biodegradable tissue engineering scaffolds. Biotechnol Bioeng. 2003; 82:578–89. [PubMed: 12652481]
24. Park YD, Tirelli N, Hubbell JA. Photopolymerized hyaluronic acid-based hydrogels and interpenetrating networks. Biomaterials. 2003; 24:893–900. [PubMed: 12504509]
25. Shu XZ, Liu YC, Palumbo FS, Lu Y, Prestwich GD. In situ crosslinkable hyaluronan hydrogels for tissue engineering. Biomaterials. 2004; 25:1339–48. [PubMed: 14643608]
26. Yeo Y, Highley CB, Bellas E, Ito T, Marini R, Langer R, et al. In situ cross-linkable hyaluronic acid hydrogels prevent post-operative abdominal adhesions in a rabbit model. Biomaterials. 2006; 27:4698–705. [PubMed: 16750564]
27. Eldridge L, Moldobaeva A, Wagner EM. Increased hyaluronan fragmentation during pulmonary ischemia. Am J Physiol Lung Cell Mol Physiol. 2011; 301:L782–L8. [PubMed: 21821727]
28. Gao F, Liu Y, He Y, Yang C, Wang Y, Shi X, et al. Hyaluronan oligosaccharides promote excisional wound healing through enhanced angiogenesis. Matrix Biol. 2010; 29:107–16. [PubMed: 19913615]
29. Voelcker V, Gebhardt C, Averbeck M, Saalbach A, Wolf V, Weih F, et al. Hyaluronan fragments induce cytokine and metalloprotease upregulation in human melanoma cells in part by signalling via TLR4. Exp Dermatol. 2008; 17:100–7. [PubMed: 18031543]
30. Aruffo A, Stamenkovic I, Melnick M, Underhill CB, Seed B. CD44 is the principal cell surface receptor for hyaluronate. Cell. 1990; 61:1303–13. [PubMed: 1694723]
31. Sherman L, Sleeman J, Herrlich P, Ponta H. Hyaluronate receptors - key players in growth, differentiation, migration and tumor progression. Curr Opin Cell Biol. 1994; 6:726–33. [PubMed: 7530464]
32. Burdick JA, Prestwich GD. Hyaluronic acid hydrogels for biomedical applications. Adv Mater. 2011; 23:H41–H56. [PubMed: 21394792]
33. Bulpitt P, Aeschlimann D. New strategy for chemical modification of hyaluronic acid: preparation of functionalized derivatives and their use in the formation of novel biocompatible hydrogels. J Biomed Mater Res. 1999; 47:152–69. [PubMed: 10449626]
34. Oh EJ, Park K, Kim KS, Kim J, Yang JA, Kong JH, et al. Target specific and long-acting delivery of protein, peptide, and nucleotide therapeutics using hyaluronic acid derivatives. J Control Release. 2010; 141:2–12. [PubMed: 19758573]
35. Chung C, Burdick JA. Influence of three-dimensional hyaluronic acid microenvironments on mesenchymal stem cell chondrogenesis. Tissue Eng Part A. 2009; 15:243–54. [PubMed: 19193129]
36. Gerecht S, Burdick JA, Ferreira LS, Townsend SA, Langer R, Vunjak-Novakovic G. Hyaluronic acid hydrogel for controlled self-renewal and differentiation of human embryonic stem cells. Proc Natl Acad Sci U S A. 2007; 104:11298–303. [PubMed: 17581871]
37. Kim J, Park Y, Tae G, Lee KB, Hwang CM, Hwang SJ, et al. Characterization of low-molecular-weight hyaluronic acid-based hydrogel and differential stem cell responses in the hydrogel microenvironments. J Biomed Mater Res A. 2009; 88A:967–75. [PubMed: 18384163]
38. Pan LJ, Ren YJ, Cui FZ, Xu QY. Viability and differentiation of neural precursors on hyaluronic acid hydrogel scaffold. J Neurosci Res. 2009; 87:3207–20. [PubMed: 19530168]
39. Lei Y, Gojgini S, Lam J, Segura T. The spreading, migration and proliferation of mouse mesenchymal stem cells cultured inside hyaluronic acid hydrogels. Biomaterials. 2011; 32:39–47. [PubMed: 20933268]
40. Kim J, Park Y, Tae G, Lee KB, Hwang SJ, Kim IS, et al. Synthesis and characterization of matrix metalloprotease sensitive-low molecular weight hyaluronic acid based hydrogels. J Mater Sci Mater Med. 2008; 19:3311–8. [PubMed: 18496734]
41. Lungwitz U, Breunig M, Blunk T, Gopferich A. Polyethylenimine-based non-viral gene delivery systems. Eur J Pharm Biopharm. 2005; 60:247–66. [PubMed: 15939236]
42. Godbey W, Wu KK, Mikos AG. Tracking the intracellular path of poly (ethylenimine)/DNA complexes for gene delivery. Proc Natl Acad Sci U S A. 1999; 96:5177–81. [PubMed: 10220439]

43. Godbey WT, Wu KK, Mikos AG. Poly(ethylenimine) and its role in gene delivery. J Control Release. 1999; 60:149–60. [PubMed: 10425321]
44. Abdallah B, Hassan A, Benoist C, Goula D, Behr JP, Demeneix BA. A powerful nonviral vector for in vivo gene transfer into the adult mammalian brain: polyethylenimine. Hum Gene Ther. 1996; 7:1947–54. [PubMed: 8930654]
45. Wang S, Ma N, Gao SJ, Yu H, Leong KW. Transgene expression in the brain stem effected by intramuscular injection of polyethylenimine/DNA complexes. Mol Ther. 2001; 3:658–64. [PubMed: 11356070]
46. Gautam A, Densmore CL, Golunski E, Xu B, Waldrep JC. Transgene expression in mouse airway epithelium by aerosol gene therapy with PEI-DNA complexes. Mol Ther. 2001; 3:551–6. [PubMed: 11319917]
47. Kichler A, Chillon M, Leborgne C, Danos O, Frisch B. Intranasal gene delivery with a polyethylenimine-PEG conjugate. J Control Release. 2002; 81:379–88. [PubMed: 12044576]
48. Rudolph C, Schillinger U, Plank C, Gessner A, Nicklaus P, Muller RH, et al. Nonviral gene delivery to the lung with copolymer-protected and transferrin-modified polyethylenimine. Biochim Biophys Acta. 2002; 1573:75–83. [PubMed: 12383945]
49. Wiseman JW, Goddard CA, McLelland D, Colledge WH. A comparison of linear and branched polyethylenimine (PEI) with DCChol/DOPE liposomes for gene delivery to epithelial cells in vitro and in vivo. Gene Ther. 2003; 10:1654–62. [PubMed: 12923564]
50. Kleemann E, Jekel N, Dailey LA, Roesler S, Fink L, Weissmann N, et al. Enhanced gene expression and reduced toxicity in mice using polyplexes of low-molecular-weight poly(ethylene imine) for pulmonary gene delivery. J Drug Target. 2009; 17:638–51. [PubMed: 19589123]
51. Segura T, Schmokel H, Hubbell JA. RNA interference targeting hypoxia inducible factor 1[alpha] reduces post-operative adhesions in rats. J Surg Res. 2007; 141:162–70. [PubMed: 17561118]
52. Wong SP, Argyros O, Howe SJ, Harbottle RP. Systemic gene transfer of polyethylenimine (PEI)-plasmid DNA complexes to neonatal mice. J Control Release. 2011; 150:298–306. [PubMed: 21192993]
53. Aoki K, Furuhata S, Hatanaka K, Maeda M, Remy JS, Behr JP, et al. Polyethylenimine-mediated gene transfer into pancreatic tumor dissemination in the murine peritoneal cavity. Gene Ther. 2001; 8:508–14. [PubMed: 11319617]
54. Coll JL, Chollet P, Brambilla E, Desplanques D, Behr JP, Favrot M. In vivo delivery to tumors of DNA complexed with linear polyethylenimine. Hum Gene Ther. 1999; 10:1659–66. [PubMed: 10428211]
55. Iwai M, Harada Y, Tanaka S, Muramatsu A, Mori T, Kashima K, et al. Polyethylenimine-mediated suicide gene transfer induces a therapeutic effect for hepatocellular carcinoma in vivo by using an Epstein-Barr virus-based plasmid vector. Biochem Biophys Res Commun. 2002; 291:48–54. [PubMed: 11829460]
56. Lei P, Padmashali RM, Andreadis ST. Cell-controlled and spatially arrayed gene delivery from fibrin hydrogels. Biomaterials. 2009; 30:3790–9. [PubMed: 19395019]
57. Kong HJ, Kim ES, Huang YC, Mooney DJ. Design of biodegradable hydrogel for the local and sustained delivery of angiogenic plasmid DNA. Pharm Res. 2008; 25:1230–8. [PubMed: 18183476]
58. Fukunaka Y, Iwanaga K, Morimoto K, Kakemi M, Tabata Y. Controlled release of plasmid DNA from cationized gelatin hydrogels based on hydrogel degradation. J Control Release. 2002; 80:333–43. [PubMed: 11943409]
59. Jang JH, Houchin TL, Shea LD. Gene delivery from polymer scaffolds for tissue engineering. Expert Rev Med Devices. 2004; 1:127–38. [PubMed: 16293016]
60. Wieland JA, Houchin-Ray TL, Shea LD. Non-viral vector delivery from PEG-hyaluronic acid hydrogels. J Control Release. 2007; 120:233–41. [PubMed: 17582640]
61. Lei Y, Segura T. DNA delivery from matrix metalloproteinase degradable poly(ethylene glycol) hydrogels to mouse cloned mesenchymal stem cells. Biomaterials. 2009; 30:254–65. [PubMed: 18838159]
62. Lei Y, Ng QKT, Segura T. Two and three-dimensional gene transfer from enzymatically degradable hydrogel scaffolds. Microsc Res Tech. 2010; 73:910–7. [PubMed: 20232458]

63. Gojgini S, Tokatlian T, Segura T. Utilizing cell-matrix interactions to modulate gene transfer to stem cells inside hyaluronic acid hydrogels. Mol Pharm. 2011; 8:1582–91. [PubMed: 21823632]
64. Lei Y, Huang S, Sharif-Kashani P, Chen Y, Kavehpour P, Segura T. Incorporation of active DNA/cationic polymer polyplexes into hydrogel scaffolds. Biomaterials. 2010; 31:9106–16. [PubMed: 20822811]
65. Lei Y, Rahim M, Ng Q, Segura T. Hyaluronic acid and fibrin hydrogels with concentrated DNA/PEI polyplexes for local gene delivery. J Control Release. 2011; 153:255–61. [PubMed: 21295089]
66. Shepard JA, Virani FR, Goodman AG, Gossett TD, Shin S, Shea LD. Hydrogel macroporosity and the prolongation of transgene expression and the enhancement of angiogenesis. Biomaterials. 2012; 33:7412–21. [PubMed: 22800542]
67. Tokatlian T, Cam C, Siegman SN, Lei Y, Segura T. Design and characterization of microporous hyaluronic acid hydrogels for in vitro gene transfer to mMSCs. Acta Biomater. 2012; 8:3921–31. [PubMed: 22820309]
68. Schrementi ME, Ferreira AM, Zender C, DiPietro LA. Site-specific production of TGF-β in oral mucosal and cutaneous wounds. Wound Repair Regen. 2008; 16:80–6. [PubMed: 18086295]
69. Szpaderska AM, Zuckerman JD, DiPietro LA. Differential injury responses in oral mucosal and cutaneous wounds. J Dent Res. 2003; 82:621–6. [PubMed: 12885847]
70. Carmeliet P, Jain RK. Molecular mechanisms and clinical applications of angiogenesis. Nature. 2011; 473:298–307. [PubMed: 21593862]
71. Ehrbar M, Zeisberger SM, Raeber GP, Hubbell JA, Schnell C, Zisch AH. The role of actively released fibrin-conjugated VEGF for VEGF receptor 2 gene activation and the enhancement of angiogenesis. Biomaterials. 2008; 29:1720–9. [PubMed: 18155761]
72. Moon JJ, Saik JE, Poché RA, Leslie-Barbick JE, Lee SH, Smith AA, et al. Biomimetic hydrogels with pro-angiogenic properties. Biomaterials. 2010; 31:3840–7. [PubMed: 20185173]
73. Silva EA, Mooney DJ. Spatiotemporal control of vascular endothelial growth factor delivery from injectable hydrogels enhances angiogenesis. J Thromb Haemost. 2007; 5:590–8. [PubMed: 17229044]
74. Zisch AH, Lutolf MP, Ehrbar M, Raeber GP, Rizzi SC, Davies N, et al. Cell-demanded release of VEGF from synthetic, biointeractive cell ingrowth matrices for vascularized tissue growth. FASEB J. 2003; 17:2260–2. [PubMed: 14563693]
75. Peppas NA, Hilt JZ, Khademhosseini A, Langer R. Hydrogels in biology and medicine: from molecular principles to bionanotechnology. Adv Mater. 2006; 18:1345–60.
76. Ehrbar M, Djonov VG, Schnell C, Tschanz SA, Martiny-Baron G, Schenk U, et al. Cell-demanded liberation of VEGF121 from fibrin implants induces local and controlled blood vessel growth. Circ Res. 2004; 94:1124–32. [PubMed: 15044320]

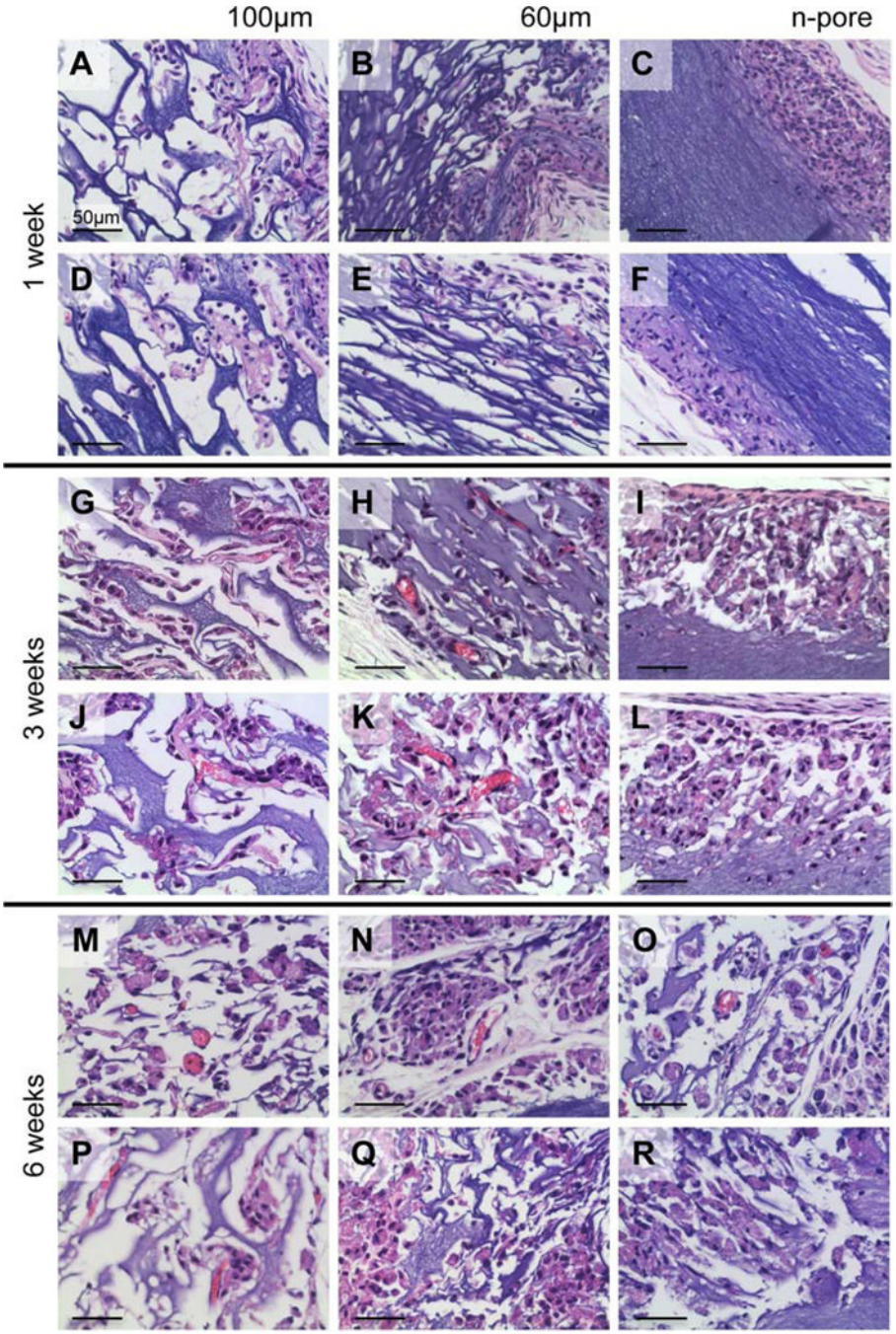

Figure 1.

H&E stained sections of 2.5 μg/μL pVEGF loaded 3.0 % HA 100 (A, G, M) and 60 μm (B, H, N) porous and n-pore (C, I, O) hydrogels at 1 (A, B, C), 3 (G, H, I), and 6 (M, N, O) weeks after subcutaneous implantation. Control pGFPluc loaded 100 (D, J, P) and 60 μm (E, K, Q) porous and n-pore (F, L, R) hydrogels at 1 (D, E, F), 3 (J, K, L), and 6 (P, Q, R) weeks exhibit relatively similar levels of cellular infiltration. Blood vessels are observed in several 100 and 60 μm porous hydrogels at 3 and 6 weeks. All images are 40× magnifications.

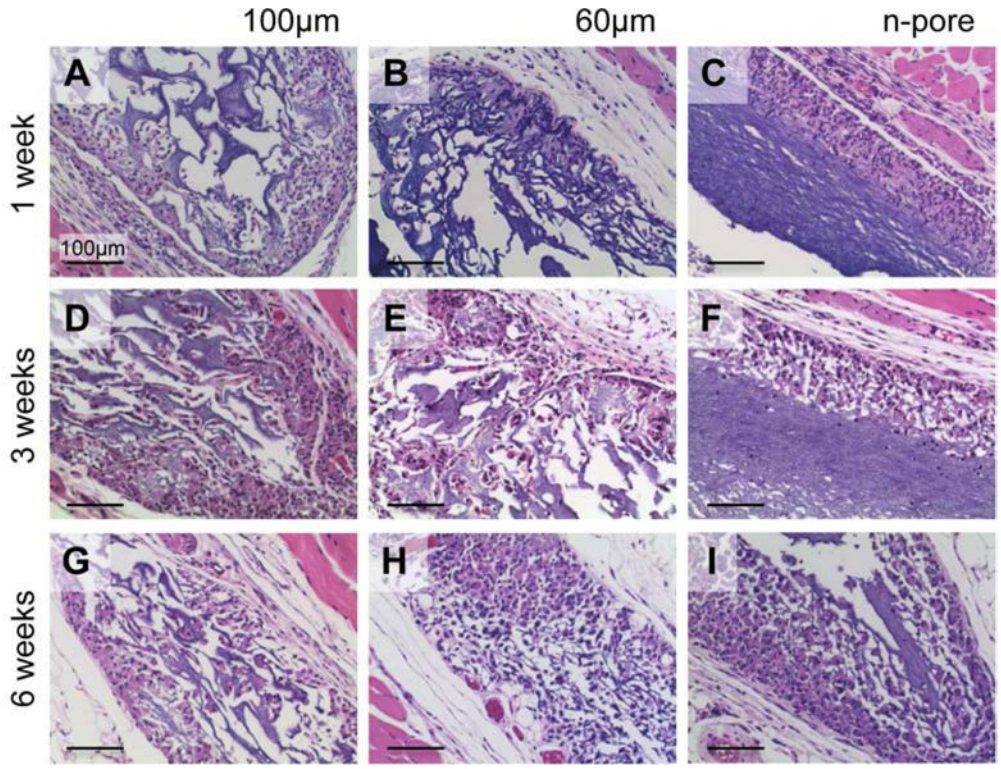

Figure 2.

H&E stained sections of polyplex loaded hydrogels and surrounding tissue to assess inflammatory response and fibrous capsule formation. 100 (A, D) and 60 μm (B, E) porous and n-pore (C, F) hydrogels at 1 (A, B, C) and 3 (D, E, F) weeks after subcutaneous implantation. All images are 20× magnifications.

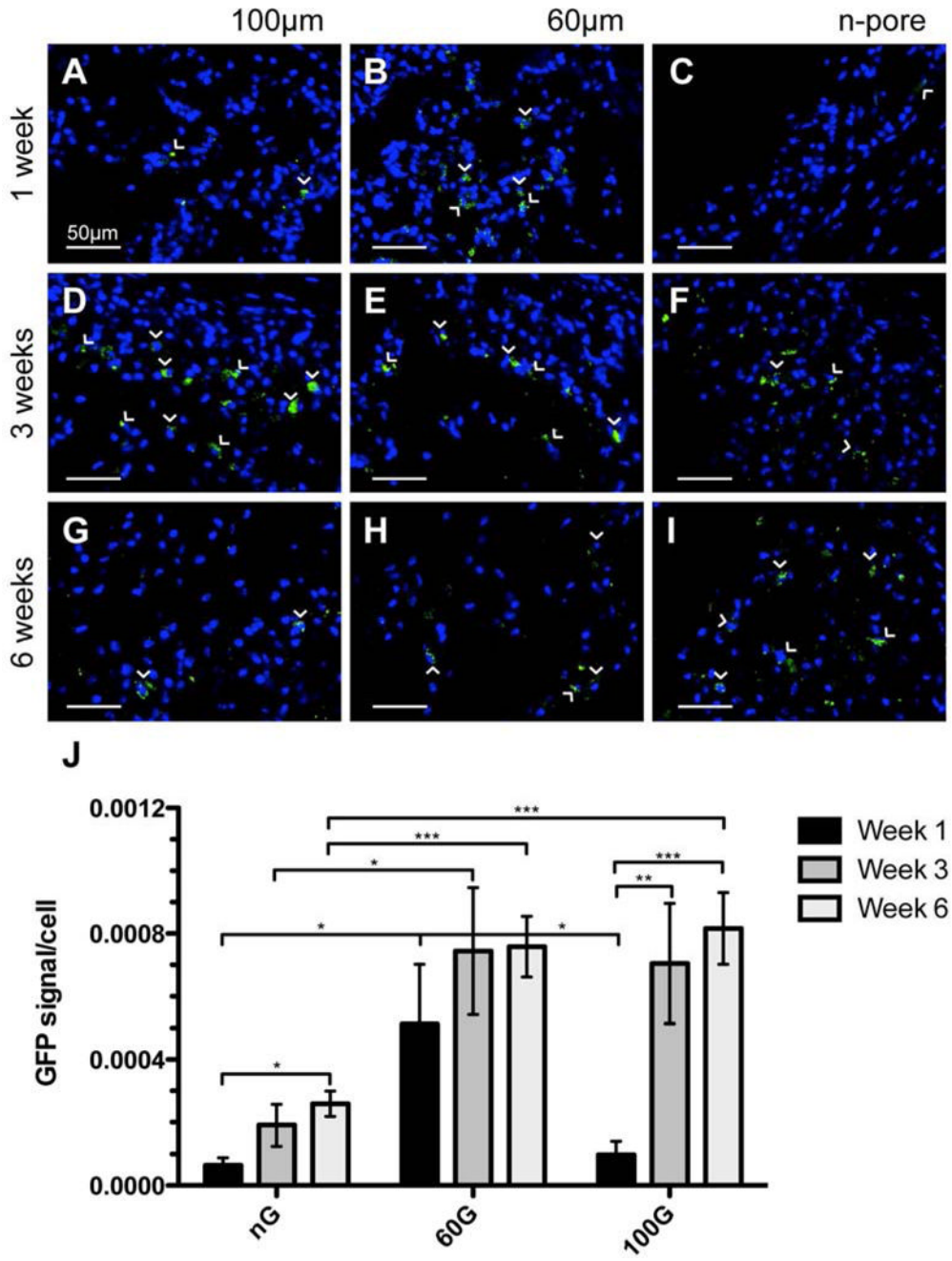

Figure 3.

Immunofluorescence staining of GFP in pGFPluc loaded control 100 (A, D, G) and 60 μm (B, E, H) porous and n-pore (C, F, I) hydrogels at 1 (A, B, C), 3 (D, E, F), and 6 (G, H, I) weeks indicates several transfected cells are present in each hydrogel over the 6 week period. Transfected cells in n-pore hydrogels, however, are only located around the hydrogel periphery where there is infiltration and gel degradation, while transfected cells in 100 and 60 μm porous gels can be found throughout. (J) Quantification of GFP positive cells normalized to total cells per image area reveals statistical differences in transfection levels at all times between 60 and 100 μm porous and n-pore hydrogels. GFP positive cells = green, cell nuclei = blue. All images are 40× magnifications.

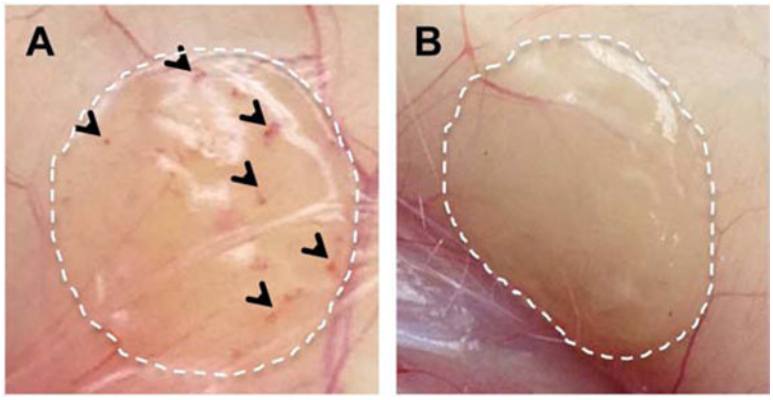

Figure 4.
Digital images of pVEGF loaded 60 μm porous (A) and n-pore (B) hydrogel implants upon excision at 6 weeks demonstrate visible differences in angiogenesis.

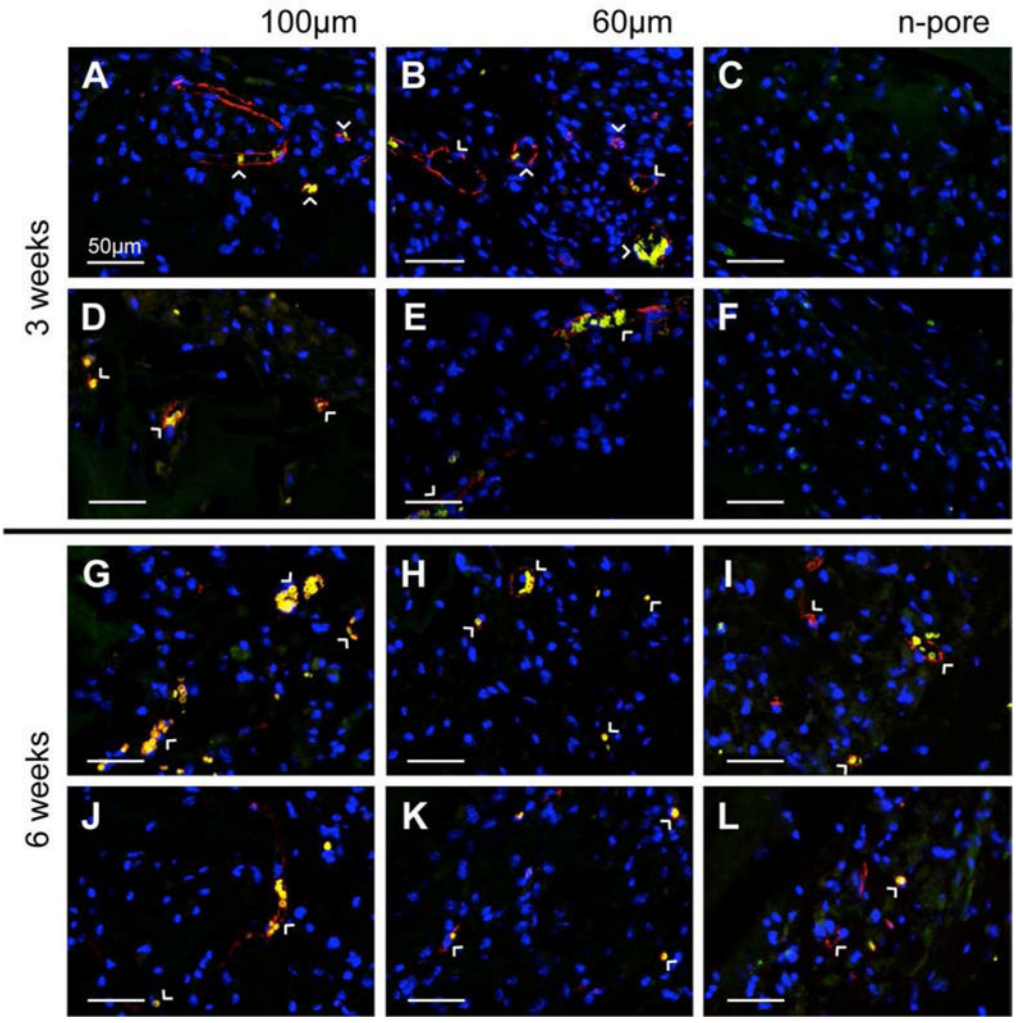

Figure 5.

Staining for endothelial markers at 3 (A-F) weeks indicated significant positive staining for 100 and 60 μm porous hydrogel implants loaded with pVEGF (A, B) and pGFPluc (D, E), respectively, and not for the n-pore implants loaded either with pVEGF (C) or pGFPluc (F). By 6 weeks (G-L), positive staining for endothelial markers was present in most implants, including 100 and 60 μm porous and several n-pore hydrogels loaded both with pVEGF (G-I) and pGFPluc (J-L), respectively. Red = PECAM positive staining = endothelial cells, yellow = erythrocytes, blue = cell nuclei. All images are 40× magnifications.

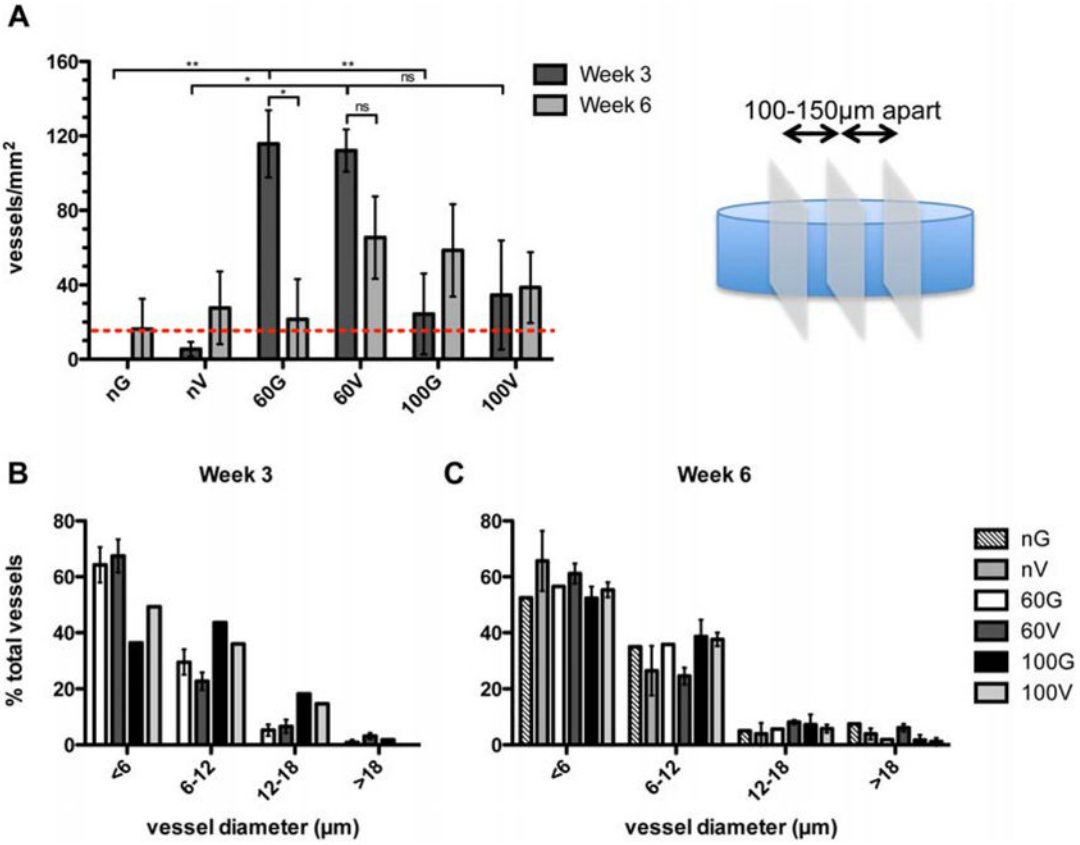

Figure 6.

Vessel quantification and characterization. (A) Vessels in 30 images over 3 sections separated by 100 – 150 μm were quantified and normalized to the total image area. The bar graph represents the average of 4 separate implants (i.e. animals). For those hydrogel implants that contained vessels (above dotted red line), vessel diameters were measured. At 3 (B) and 6 (C) weeks approximately 50 % of vessels in all implants were less than 6 μm in diameter. G = pGFPluc, V = pVEGF loaded hydrogels.

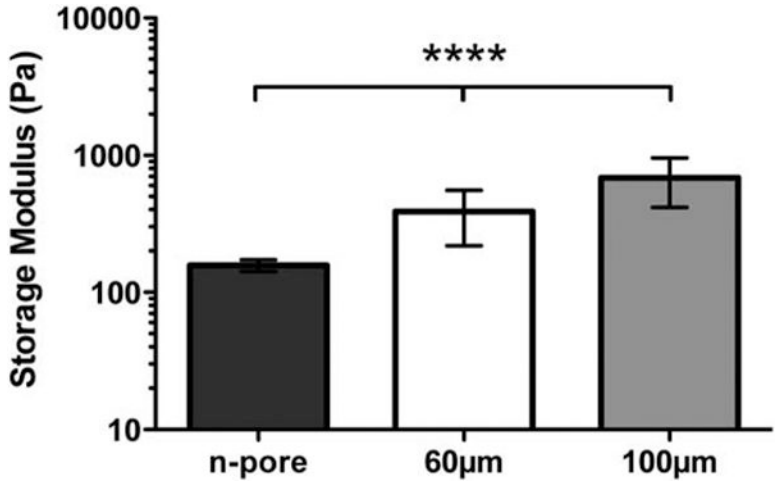

Figure 7.

Hydrogel mechanical properties were determined using plate-to-plate rheometry. Average storage modulus under a constant strain of 0.01 and frequency range of 0.1-10 Hz are shown for various pore size hydrogels.

Table 1

Summary of hydrogel implants that were positive for blood vessels. Positive hydrogel implants contained a minimum of 15 vessels/mm^2, which corresponded to at least 1 vessel in 50 % of sections. G = pGFPluc, V = pVEGF loaded hydrogels.

Hydrogel type	Implants positive for vessels	
	Week 3	Week 6
nG	0/4	1/4
nV	0/3	2/4
60G	4/4	1/4
60V	4/4	3/4
100G	1/4	2/3
100V	1/4	3/4